

Reference-free fatigue crack detection using deep long short-term memory network (DLSTM) and nonlinear ultrasonic modulation

Jinho Jang ^a, Peipei Liu ^{a,b}, Ohjun Kwon ^a, Jaemook Choi ^a, Zhanxiong Ma ^a, Hoon Sohn ^{a,b,*}

^a Department of Civil and Environmental Engineering, Korea Advanced Institute of Science and Technology, Daejeon, 34141, South Korea

^b Center for 3D Printing Nondestructive Testing, Korea Advanced Institute of Science and Technology, Daejeon, 34141, South Korea

ARTICLE INFO

Keywords:

Nonlinear ultrasonic modulation
Deep long short-term memory network
Fatigue crack detection
Submerged structure
Deep learning
Reference-free

ABSTRACT

Nonlinear ultrasonic modulation is sensitive to fatigue crack, but a reference signal or user-specified threshold is often required for crack diagnosis, easily causing false alarms in noisy environments. In this study, a reference-free damage detection method was developed by applying a deep long short-term memory network (DLSTM) to nonlinear ultrasonic modulation signals. First, an ultrasonic signal was generated and measured using piezo-ceramic ultrasonic transducers. Subsequently, a DLSTM network was constructed and trained to learn the inherent sequential patterns of the measured ultrasonic signals. Then, an absolute damage index (ADI) was defined and computed using only the current ultrasonic signal without any reference ultrasonic signal obtained from the intact condition. Finally, the crack was automatically detected using the ADI and without any user-specified threshold. The performance of the proposed method was examined using data from a submerged floating tunnel model and an actual long-span bridge. The results highlight the feasibility of the proposed method for automatic fatigue crack detection.

1. Introduction

Fatigue crack detection is essential for monitoring a wide range of mechanical, aerospace, and civil structures. Fatigue cracks are one of the main causes of failure of metallic structures, and 90% of metallic structure failures are attributed to fatigue cracks [1]. Therefore, early detection of fatigue cracks is important to prevent catastrophic failure of structures. However, a fatigue crack often remains undetectable until it reaches approximately 80% of its fatigue life [2].

Several structural health monitoring (SHM) and nondestructive evaluation (NDE) techniques have been developed for fatigue crack detection, such as X-ray imaging, magnetic particle inspection, ultrasonics, thermography, acoustic emission, and electromagnetics [3–8]. Among these techniques, nonlinear ultrasonic techniques utilizing harmonics, modulation, and sub-harmonics are gaining popularity owing to their high sensitivity to crack [9–12]. In particular, a nonlinear ultrasonic modulation technique is promising because it is highly sensitive to microcracks and minimally influenced by other types of nonlinearity, such as circuit nonlinearity [12].

Nonlinear ultrasonic modulation is produced by the nonlinear interaction of two distinct waves with different frequencies when they

propagate through a crack [13]. Nonlinear ultrasonic modulation has been used to detect cracks in welded joints, rotating steel shafts, silicon wafers, and aluminum plate [14–17]. Cracks are often identified by comparing the amplitudes of the nonlinear modulation components obtained before and after the crack formation. Because of this dependency on the reference data obtained from the pristine condition, existing modulation techniques are often prone to false alarms because of signal variations irrelevant to the crack.

Recently, a reference-free technique was developed for crack detection using nonlinear ultrasonic modulation [18]. In this technique, a crack is detected when the spectral amplitude of the nonlinear ultrasonic modulation exceeds a threshold value determined by current noise level of the ultrasonic signal, rather than the prior baseline signal. However, this technique requires a user-specified threshold for crack detection. Additionally, because the threshold value is a function of the noise level, the performance and reliability of crack detection can be affected by the noise level.

Furthermore, existing nonlinear ultrasonic modulation-based crack detection techniques have technical hurdles in their application to offshore underwater structures. Because of the harsh conditions, underwater states are noisy environments, and ultrasonic waves leak into

* Corresponding author. Department of Civil and Environmental Engineering, Korea Advanced Institute of Science and Technology, Daejeon, 34141, South Korea.
E-mail address: hoonsohn@kaist.ac.kr (H. Sohn).



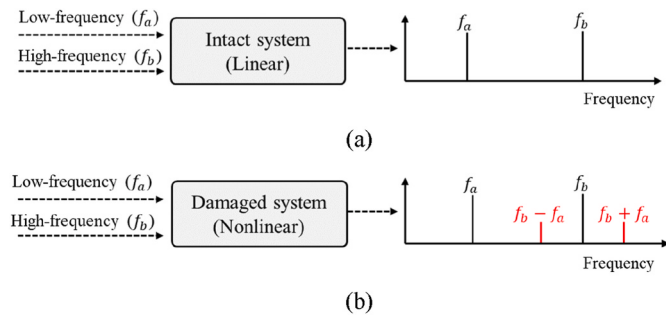


Fig. 1. Illustration of nonlinear ultrasonic modulation, (a) Intact (linear) case, and (b) Damaged (nonlinear) case.

the water, weakening ultrasonic signals, including modulation components [19].

Based on the authors' previous work to use long short-term memory network (LSTM) for noise reduction in ultrasonic signal [20], this study further improves the method and presents a deep long short-term memory network (DLSTM)-based fatigue crack detection technique so that fatigue cracks can be detected solely based on the instantaneous measurement of ultrasonic signals without any prior baseline signals or user-specified thresholding. The uniqueness of this study includes the following: (1) Reference-free crack diagnosis using only current ultrasonic signal without any reference signal obtained from the intact condition; (2) Online instantaneous training of the DLSTM network to extract the inherent sequential features induced by a crack without accumulation of past training data; (3) Automatic crack diagnosis without any user-specified threshold for decision making; and (4) Improved crack detection performance under noisy under-water and real field environments.

The remainder of this study is organized as follows. Section 2 presents the background of this study. Section 3 describes the crack-detection algorithm based on DLSTM and nonlinear ultrasonic

modulation. Sections 4 and 5 present the experimental setup and test results obtained from submerged floating tunnel and real bridge tests, respectively. Finally, the conclusions and summaries are presented in Section 6.

2. Research background

2.1. Working principle of nonlinear ultrasonic modulation

When two sinusoidal signals with distinctive frequencies, f_a and f_b propagate in an intact system, as shown in Fig. 1(a), the system response contains only the frequency components corresponding to f_a and f_b . On the other hand, once the system behaves nonlinearly owing to a crack, the system response contains not only the linear components at f_a and f_b but also their modulation components at $f_b \pm f_a$, as illustrated in Fig. 1(b). This mechanism is known as nonlinear ultrasonic modulation [21, 22]. Because this mechanism occurs only in the presence of nonlinearity in the system, ultrasonic modulation components can be indicators of cracks. Considering only the first-order nonlinear ultrasonic modulation components at $f_b \pm f_a$, their amplitudes, m_{\pm} , are proportional to the amplitudes at f_a and f_b [22].

$$m_{\pm} \propto \beta_{a,b}^{\pm} ab \quad (1)$$

where $\beta_{a,b}^{\pm}$ are the nonlinear coefficients at $f_b \pm f_a$, and a and b are the amplitudes of the linear responses at f_a and f_b , respectively. However, the amplitudes of the modulation components are often much smaller than those of the linear components and are buried under noise.

2.2. Deep long short-term memory (DLSTM) model

LSTM is a type of recurrent neural network (RNN) and is widely used for training sequential data with long-term dependencies [23,24]. As shown in Fig. 2, each memory cell is composed of an input gate, output gate, forget gate, and self-recurrent neuron. The computations of the

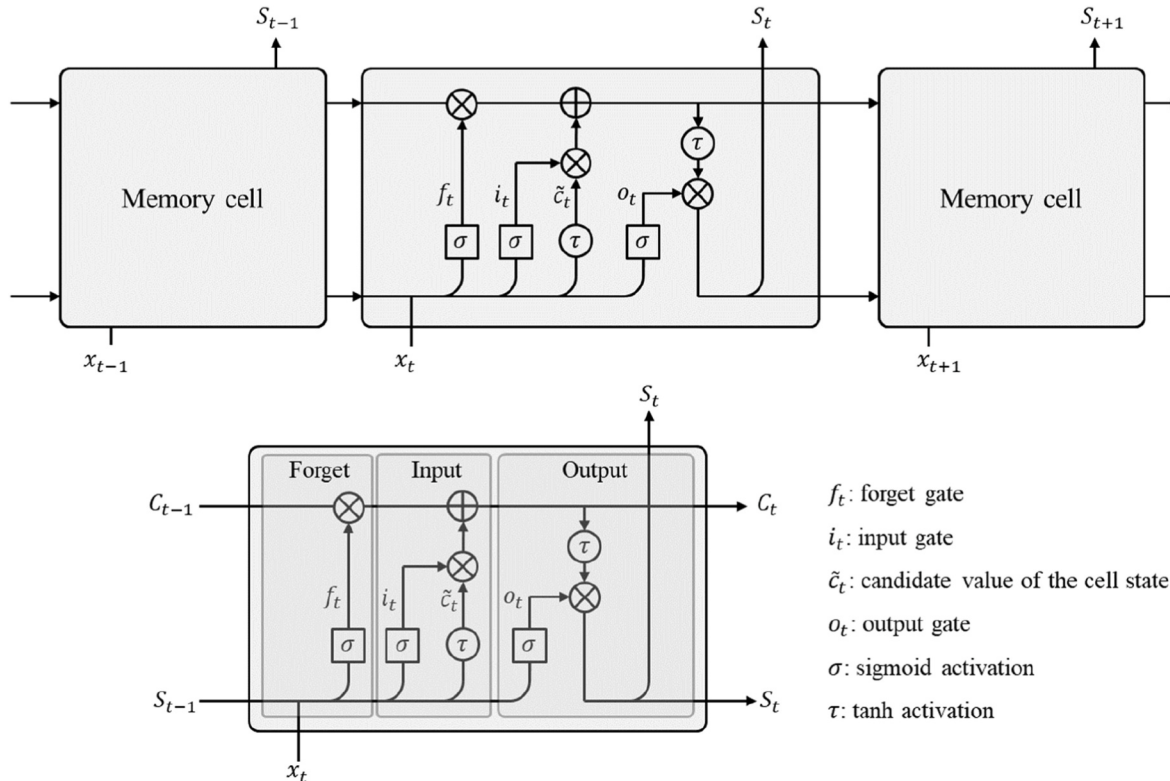


Fig. 2. Overview of long short-term memory (LSTM) network.

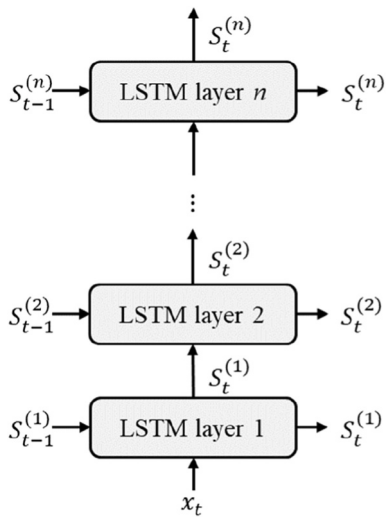


Fig. 3. Architecture of deep long short-term memory (DLSTM) network.

LSTM memory cell are expressed as follows [25]:

$$f_t = \sigma(X_t U^f + S_{t-1} W^f + b^f) \quad (2)$$

$$i_t = \sigma(X_t U^i + S_{t-1} W^i + b^i) \quad (3)$$

$$\tilde{c}_t = \tau(X_t U^c + S_{t-1} W^c + b^c) \quad (4)$$

$$C_t = C_{t-1} \otimes f_t \oplus i_t \otimes \tilde{c}_t \quad (5)$$

$$o_t = \sigma(X_t U^o + S_{t-1} W^o + b^o) \quad (6)$$

$$S_t = o_t \otimes \tau(C_t) \quad (7)$$

where U , W and b are the weights of the input, recurrent, and bias, respectively. The superscripts i , o , f and c represent the input gate, output gate, forget gate, and self-recurrent neuron, respectively. x_t is the sequential input data at the t th time. S_t , C_t , \tilde{C}_t are the hidden state, cell state, and new candidate values of the cell state, respectively. Finally, σ , τ , \oplus , and \otimes are sigmoid activation function, hyperbolic tangent (tanh) activation function, pointwise addition and multiplication operators, respectively.

It has been reported that increasing the depth of an LSTM network improves its overall performance [26]. A DLSTM network has been developed for effective time series training owing to its improved learning abilities for deep network architectures [27]. In the DLSTM architecture, multiple LSTM layers were stacked, as shown in Fig. 3. The goal of stacking multiple LSTM layers is to estimate features at the lower layers and train these representations progressively at the higher layers. The advantage of the deep architecture is that each layer can process a portion of the assigned task and subsequently pass it to the next layer until the last layer provides the output. In addition, this deep architecture allows the hidden state in each layer to operate at different time-scales for effective training [28]. Because of these advantages, the deep architecture can train long-term dependency data, such as ultrasonic signals, better than shallow architecture [28,29].

3. Development of a reference-free fatigue crack detection technique

Fig. 4 shows an overview of the proposed reference-free fatigue crack detection algorithm based on DLSTM and nonlinear ultrasonic modulation. The proposed algorithm is explained step-by-step as follows.

Step 1: Instantaneous training of DLSTM

When two ultrasonic inputs at f_a and f_b are applied to an intact structure, the structural response can be written as [30]:

$$x(t) = a(t)e^{i2\pi f_a t} + b(t)e^{i2\pi f_b t} + u_s(t) \quad (8)$$

where $a(t)$ and $b(t)$ are the amplitudes of the linear responses at f_a and f_b , and $u_s(t)$ is the amplitude of white noise and $u_s(t)$ is randomly distributed in the time domain. When a fatigue crack exists, additional nonlinear modulation components appear at $f_b \pm f_a$ as follows:

$$x(t) = a(t)e^{i2\pi f_a t} + b(t)e^{i2\pi f_b t} + m_-(t)e^{i2\pi(f_b-f_a)t} + m_+(t)e^{i2\pi(f_b+f_a)t} + u_s(t) \quad (9)$$

where $m_-(t)$ and $m_+(t)$ are the amplitudes of the nonlinear ultrasonic modulation components at $f_b \pm f_a$. A DLSTM network is constructed and trained to learn the inherent sequential patterns out of the current response signal, considering $e^{i2\pi f_t}$ (i.e., $e^{i2\pi f_a t}$, $e^{i2\pi f_b t}$, and $e^{i2\pi(f_b \pm f_a)t}$) exhibits periodic patterns in the time domain. Note that the noise component $u_s(t)$ has no features that the network can learn along the time series because $u_s(t)$ is randomly distributed in the time domain.

For instantaneous training of the DLSTM network, the current ultrasonic signal $x_t = (x_1, x_2, \dots, x_T)$ ($0 \leq t \leq T$) is normalized to have zero mean and unit variance. The DLSTM network consists of a sequence input layer, LSTM layers, a fully connected layer, and an output layer. The LSTM layer consists of memory cells, associated gate units, and hidden units that determine how much information is learned by the layer. To learn the inherent sequential patterns that are periodically repeated, the DLSTM network is trained using predictors $P = (x_1, x_2, \dots, x_{t-1})$, and the target responses, $Y = (x_2, x_3, \dots, x_t)$. As shown in Fig. 4, the hidden state at time t , $S_t^{(1)}$, is first calculated using Eqs. (2)–(7), and proceeds upward to the second LSTM layer. This process continues until the last LSTM layer is compiled in the network to learn the one-step advanced signal at time $t+1$ ($S_t^{(n)} = \hat{x}_{t+1}$). Subsequently, the proposed DLSTM network is trained to predict the next sequence of data points of the ultrasonic signal while only containing the inherent pattern of the signal.

Step 2: Multi-time step denoised ultrasonic response prediction

The entire current ultrasonic signal x_t ($0 \leq t \leq T$) is fed into the trained DLSTM network to predict the following sequence data point of the ultrasonic signal \hat{x}_t , and to repetitively update the network state using the predicted \hat{x}_t , thus achieving a predicted signal sequence \hat{x}_t ($\hat{t} > T$). In the damaged case, the predicted \hat{x}_t contains only sequentially repeated components $e^{i2\pi f_a}$, $e^{i2\pi f_b}$, and $e^{i2\pi(f_b \pm f_a)}$. Then, x_t and the denoised \hat{x}_t are combined into vector sequences $x_{t+\hat{t}}$, as follows:

$$x_{t+\hat{t}} = [x_t, \hat{x}_t] = \begin{bmatrix} a(t)e^{i2\pi f_a t} + b(t)e^{i2\pi f_b t} + m_-(t)e^{i2\pi(f_b-f_a)t} + m_+(t)e^{i2\pi(f_b+f_a)t} + u_s(t), \\ a'(\hat{t})e^{i2\pi f_a \hat{t}} + b'(\hat{t})e^{i2\pi f_b \hat{t}} + m'_-(\hat{t})e^{i2\pi(f_b-f_a)\hat{t}} + m'_+(\hat{t})e^{i2\pi(f_b+f_a)\hat{t}} \end{bmatrix} \quad (10)$$

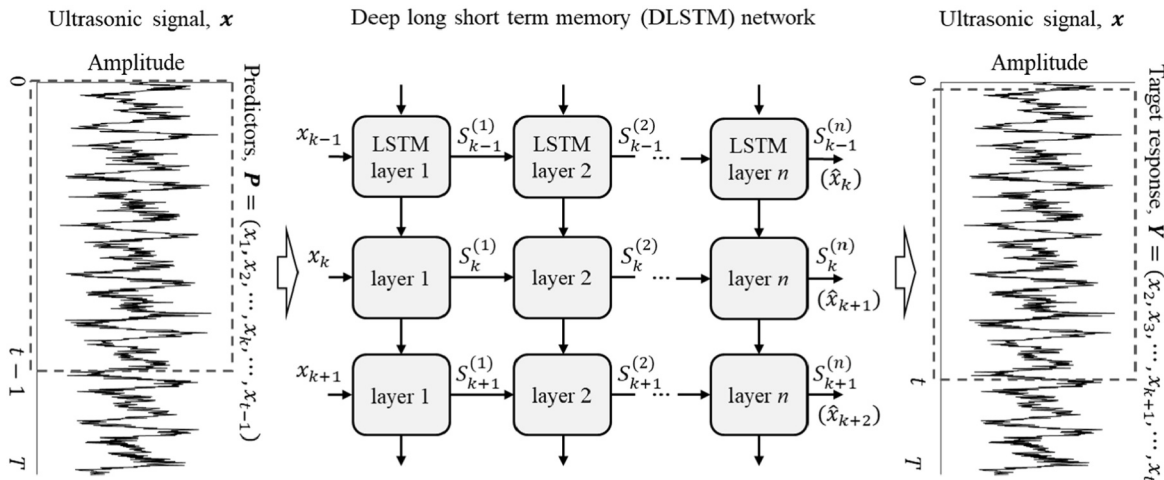
where $a'(\hat{t})$, $b'(\hat{t})$, $m'_\pm(\hat{t})$ are the amplitudes of the predicted linear response at f_a and f_b , and the amplitudes of the nonlinear ultrasonic modulation components at $f_b \pm f_a$, respectively. Eq. (10) shows that the energy of the nonlinear ultrasonic modulation components increases with respect to the length of the predicted \hat{x}_t , whereas the noise components are eliminated through time series training.

In the intact case, the nonlinear ultrasonic modulation components $e^{i2\pi(f_b \pm f_a)}$, do not exist; therefore, \hat{x}_t only contains the sequentially repeated components of $e^{i2\pi f_a}$ and $e^{i2\pi f_b}$, and the combined signal can be written as:

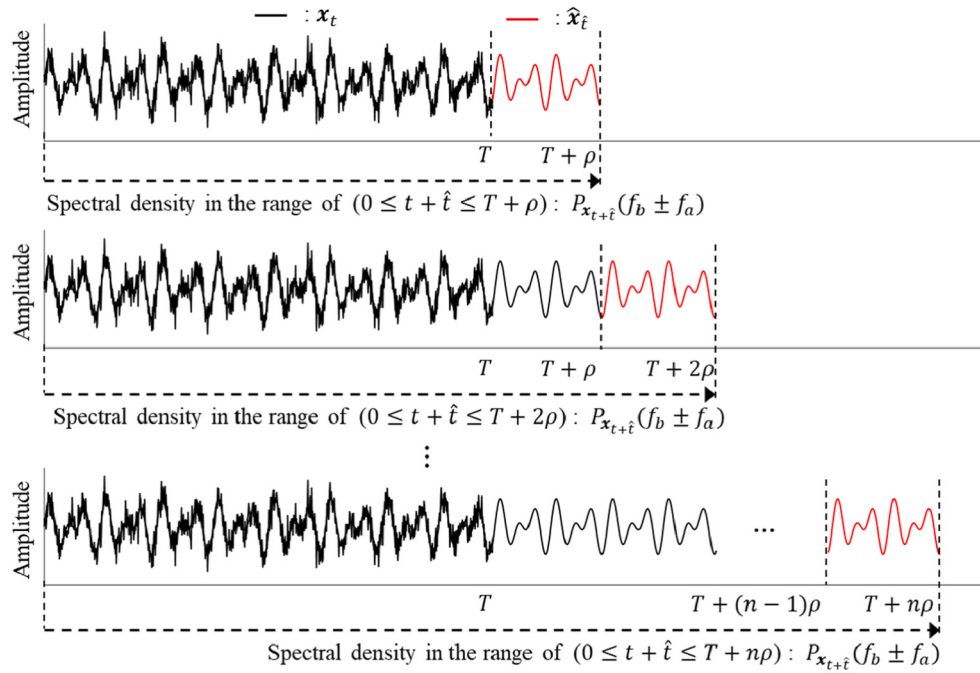
$$x_{t+\hat{t}} = [x_t, \hat{x}_t] = [a(t)e^{i2\pi f_a t} + b(t)e^{i2\pi f_b t} + u_s(t), a'(\hat{t})e^{i2\pi f_a \hat{t}} + b'(\hat{t})e^{i2\pi f_b \hat{t}}] \quad (11)$$

Note that the signal components at $f_b \pm f_a$ are also noise, because there are no nonlinear ultrasonic modulation components. Eq. (11)

Step 1. Instantaneous training of DLSTM



Step 2. Multi-time step denoised ultrasonic response prediction



Step 3. Reference-free fatigue crack diagnosis

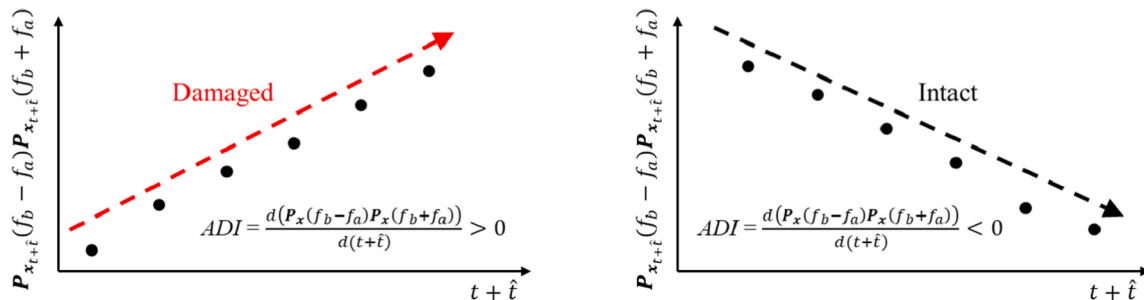


Fig. 4. Overview of proposed reference-free fatigue crack detection algorithm.

shows that the energy of the noise components at $f_b \pm f_a$ decreased with respect to the length of the predicted \hat{x}_t .

Here, \hat{x}_t are predicted multiple times (n times) with an increasing \hat{t} range at a time interval ρ ($T < \hat{t} \leq T + n\rho$, n is an integer excluding 0), and the corresponding spectral density values of the combined signal

$x_{t+\hat{t}}$ at $f_b \pm f_a$ are calculated.

$$P_{x_{t+\hat{t}}}(f_b \pm f_a) = X_{t+\hat{t}}(f_b \pm f_a) X_{t+\hat{t}}^*(f_b \pm f_a) \quad (12)$$

where $X(f) = \int_{-\infty}^{\infty} x e^{-j2\pi ft} dt$ and $*$ denotes the complex conjugate. The time interval of ρ is designed such that the energy of the nonlinear

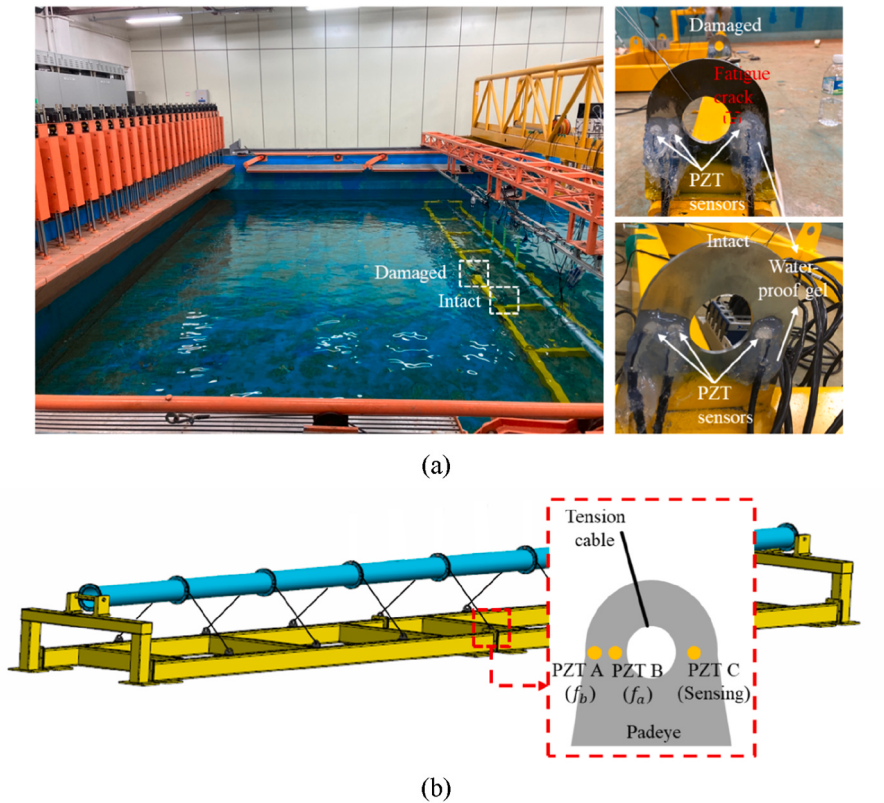


Fig. 5. Configuration of the submerged floating tunnel (SFT) model, (a) SFT and padeye structures, (b) Illustration of SFT model.

modulation components if they exist in x_t can increase noticeably in the combined signal $\hat{x}_{t+\hat{t}}$. In this study, we included 10^4 times of the period of $f_b - f_a$ for each time interval, as follows:

$$\rho = \frac{10^4}{f_b - f_a} \quad (13)$$

Step 3: Reference-free fatigue crack diagnosis

The absolute damage index (*ADI*) is defined as the rate of change of the spectral density $P_{x_{\hat{t}}} (f_b \pm f_a)$ with respect to the increased prediction time:

$$ADI = \frac{d(P_{x_{\hat{t}}} (f_b - f_a) P_{x_{\hat{t}}} (f_b + f_a))}{d(t + \hat{t})} \quad (14)$$

For a damaged case, *ADI* will always be greater than zero because the spectral density at $f_b \pm f_a$ is amplified as $\eta\rho$ increases, as illustrated in Fig. 4. On the other hand, in the intact case, noises at $f_b \pm f_a$ are eliminated in $\hat{x}_{\hat{t}}$, so the spectral density at $f_b \pm f_a$ decreases as $\eta\rho$ increases and *ADI* is less than zero. Therefore, *ADI* can be used for reference-free fatigue crack detection without any user-specified thresholding, as follows:

$$ADI > 0 \rightarrow DamageA$$

$$DI < 0 \rightarrow Intact \quad (15)$$

Here, through instantaneous training of the DLSTM network with the current ultrasonic signal x_t and multi-time step prediction of $\hat{x}_{\hat{t}}$, *ADI* can be calculated without relying on any reference data or threshold. Crack detection with the proposed *ADI* is also insensitive to signal noise because the noise components are eliminated by the trained DLSTM, and a denoised $\hat{x}_{\hat{t}}$ can be obtained.

4. Experimental validation using submerged floating tunnel model

4.1. Test configuration

A submerged floating tunnel (SFT) can be an attractive alternative to conventional long-span bridges or immersed tunnels because the construction of SFTs is not limited by the span length or depth of the ocean floor. There have been ongoing efforts to construct SFTs worldwide. As part of these efforts, interest in an SHM system to evaluate the integrity of SFTs is increasing. In particular, the detection of fatigue cracks in anchor systems is critical for the integrity and safety of SFTs.

The performance of the proposed technique was tested experimentally using an SFT model. The SFT model was submerged into a 12 m long, 10 m wide and 2 m deep ocean research basin, as shown in Fig. 5(a). The SFT was composed of eight bolt-connected aluminum tubes, with a total length of 8 m. Each tube was 1 m long and had a uniform circular cross-section with an inner diameter of 13 cm and a thickness of 0.5 cm. Stainless steel tension cables with a 0.5 mm diameter and padeyes were used to connect the SFT to the anchor system, as shown in Fig. 5(b). A total of 14 mooring cables were equally spaced at 1 m intervals along the longitudinal direction of the tunnel. Inside the basin, waves with 140 mm amplitude and 0.16 Hz frequency were generated by a wave-generator.

The padeyes used in the SFT model were made of SM490 steel, and the dimensions of the padeye specimens are shown in Fig. 6(a). The height and bottom width were 132 mm, hole radius was 22 mm, and thickness of the specimen was 5 mm. Three piezoceramic ultrasonic transducers (PZT) with a 9 mm diameter and 0.5 mm thickness (APC International, APC850) were installed on the specimen for ultrasonic generation and sensing. As shown in Fig. 6(a), PZT A and PZT B were used to create low-frequency (f_a) and high-frequency (f_b) ultrasonic signals, and PZT C was used for ultrasonic measurement. A 6 mm long and 10 μ m wide fatigue crack was created on the inner edge of the hole

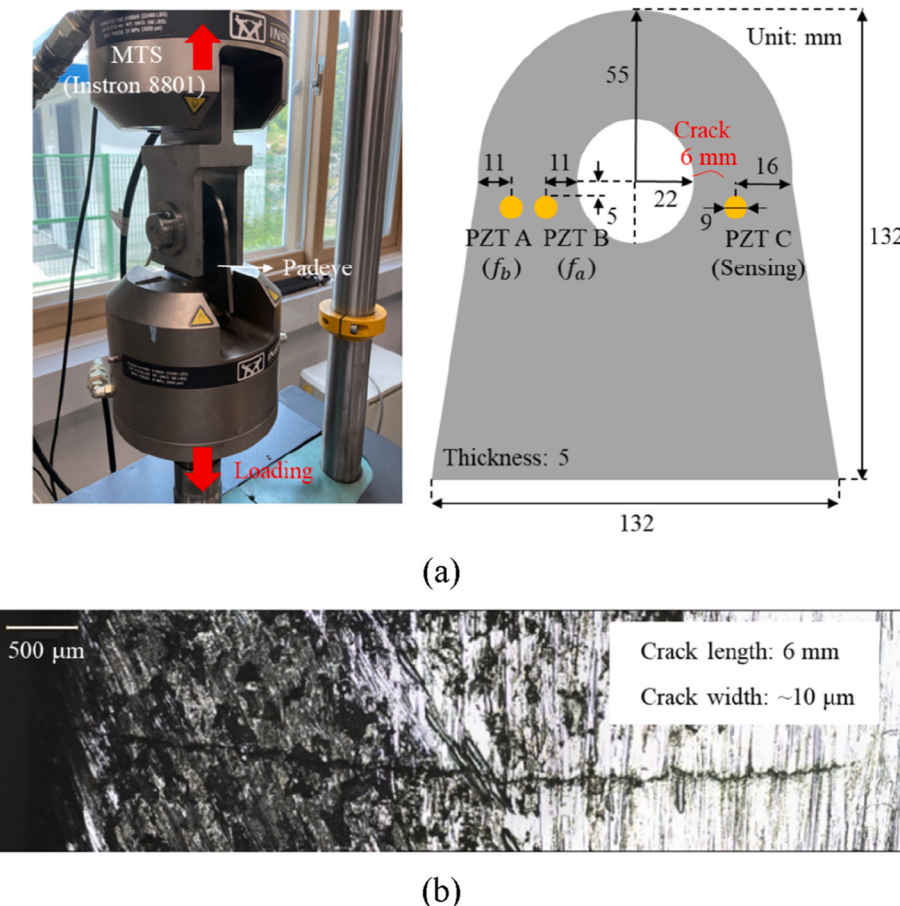


Fig. 6. (a) Geometrical descriptions of padeye with PZTs and its setup in a MTS machine, (b) Microscopy image of fatigue crack.

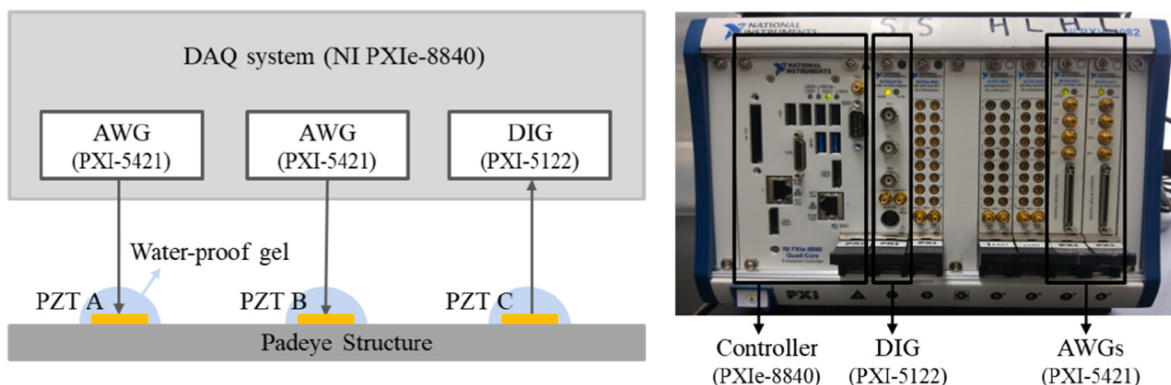


Fig. 7. Data measurement system for ultrasonic signal generation and measurement.

Table 1
Results of DLSTM network architecture optimization.

Layer	Hidden units	Batch size	Batch loss	Validation loss	Epochs
2	[100, 100]	500	0.0040	0.0029	640
3	[100, 100, 100]	500	0.0035	0.0018	560
4	[100, 100, 100, 100]	500	0.0042	0.0021	560
3	[150, 100, 100]	500	0.0031	0.0022	640
3	[150, 150, 100]	500	0.0025	0.0016	1120
3	[200, 150, 100]	500	0.0031	0.0028	400

of a padeye using an MTS machine (Instron 8801), which was then installed into the SFT model in the research basin. The amplitude of the cyclic loading created by the MTS machine varied between 6 and 60 KN, and the frequency was fixed at 10 Hz. The padeye connecting the SFT and anchor is subject to loading mode I, which is similar to its loading condition in MTS test. Therefore, it is expected that fatigue crack will occur at the same location when the padeye is installed in the SFT structure. Another reason to produce a cracked padeye beforehand was due to the large expense and time cost to create a fatigue crack directly in the SFT model. A microscopic image of a fatigue crack is shown in Fig. 6(b). One damaged and one intact padeye were tested in this experiment. DOW CORNING RTV-3145, which is a waterproof gel, was used for waterproofing PZTs. The identical test was repeated three times

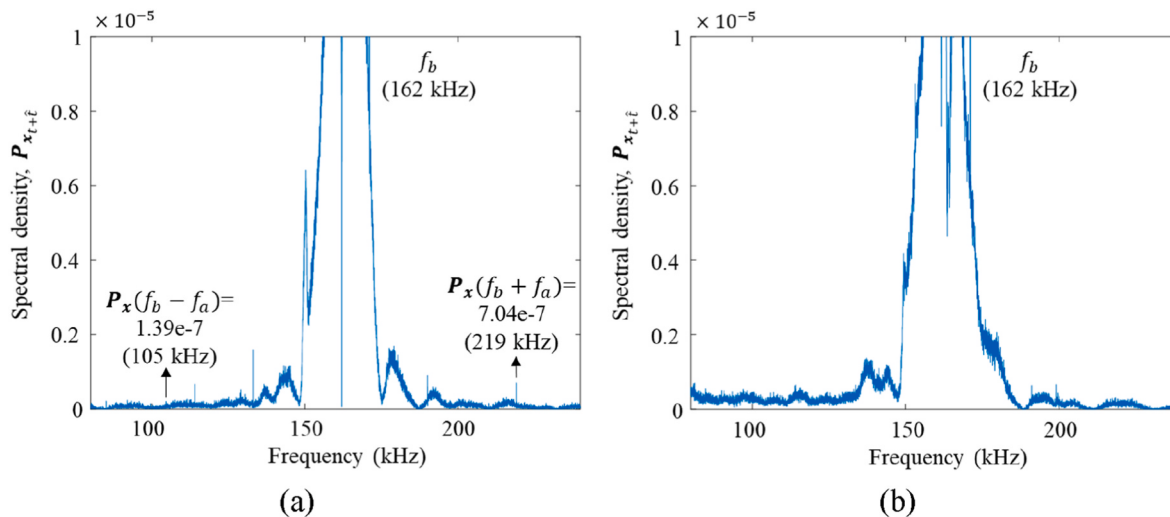


Fig. 8. Representative raw ultrasonic response signals in the frequency domain obtained in Test #1. (a) Damaged padeye, (b) Intact padeye.

Table 2
Results of fatigue crack detection in Test #1.

n	$t + \hat{t}$	$(P_{x_{t+\hat{t}}} (f_b - f_a) P_{x_{t+\hat{t}}} (f_b + f_a))_n$	
		Damaged	Intact
1	0.14	5.56e-13	2.40e-14
2	0.23	7.51e-13	1.65e-14
3	0.32	1.51e-12	1.15e-14
4	0.41	2.61e-12	8.02e-15
5	0.50	4.88e-12	5.43e-15
<i>ADI</i>		2.17e-12 <i>ADI</i> > 0	-8.33e-14 <i>ADI</i> < 0
		8.43e-12	-5.56e-14
		1.22e-11	-3.87e-14
		2.52e-11	-2.88e-14

for validation (labeled Test #1, #2, and #3).

A National Instruments PXI system consisting of a controller (PXIE-8840), two arbitrary waveform generators (AWGs, PXI-5421), and a digitizer (DIG, PXI-5122) was used for the data measurement, as shown in Fig. 7. The two AWGs created sinusoidal ultrasonic input signals at f_a

and f_b , and the duration and peak-to-peak amplitudes were set to 0.05 s and 12 V, respectively. The input frequencies were selected as $f_a = 57$ kHz and $f_b = 162$ kHz considering the local resonance characteristics of the padeye specimen and to avoid the overlap of the nonlinear modulation components with the higher-order harmonic components of the f_a input [31]. The corresponding ultrasonic response signals were obtained using the DIG with a 1 MHz sampling rate for 0.05 s.

4.2. DLSTM network construction, training, and optimization

For the DLSTM network training, the initial 90% and remaining 10% of the ultrasonic signal were divided into training (**R**) and validation (**V**) datasets. In the proposed technique, data shuffling is not considered because the inherent sequential pattern of data is crucial in this research. Half of the mean squared error ($\frac{1}{2}$ MSE) was used as the validation loss function. The validation was performed in every epoch, and early stopping, which stopped the training when the validation loss was equal to or larger than the validation loss in the previous epoch, was used to avoid the overfitting problem. The DLSTM network was trained on mini-batch stochastic optimization using an adaptive moment estimation

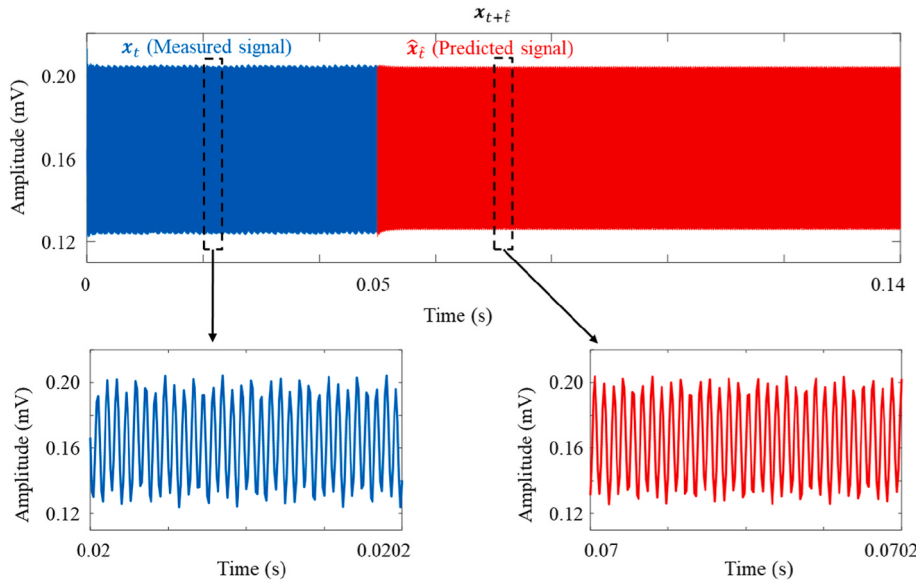


Fig. 9. Representative $x_{t+\hat{t}}$ from the damaged specimen in Test #1 when $n = 1$ ($t + \hat{t} = 0.14$).

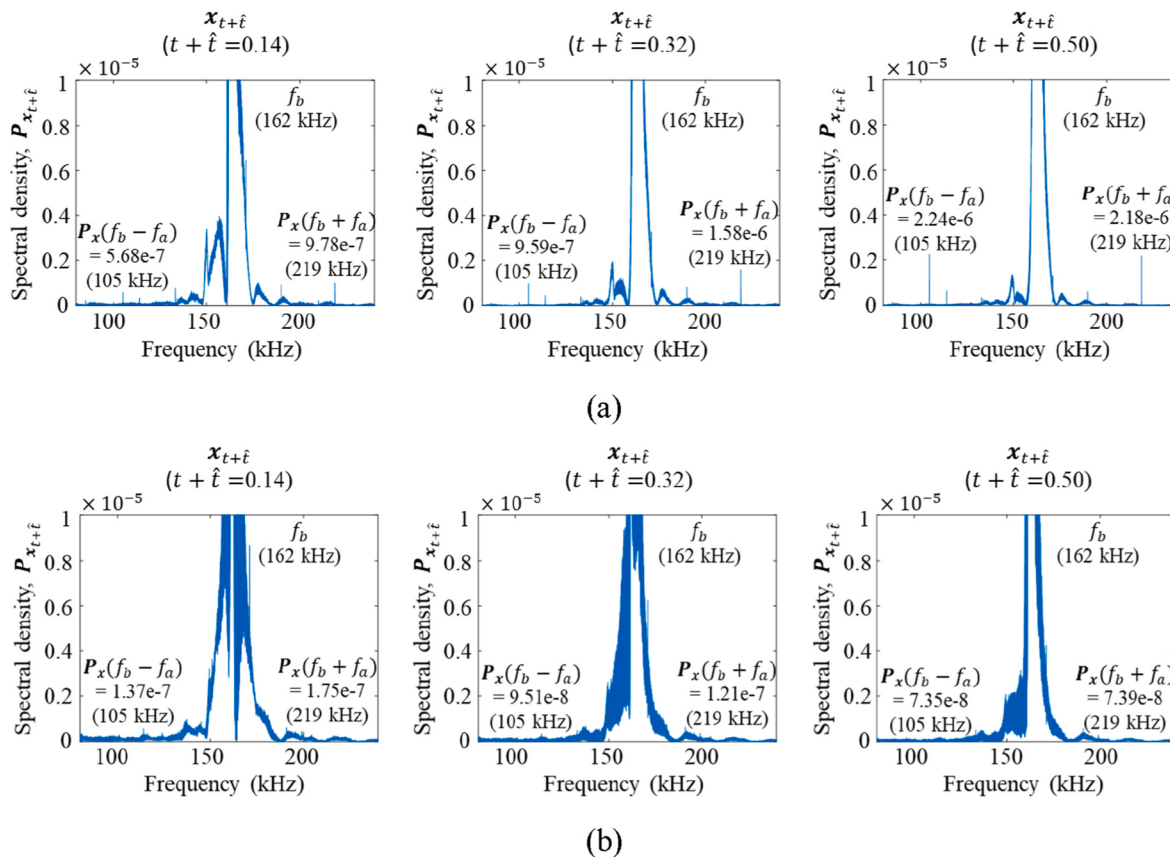


Fig. 10. Representative $P_{x,t+\hat{t}}$ calculated at three different time intervals ($t + \hat{t} = 0.14, 0.32, 0.50$) in Test #1. (a) Damaged padeye, (b) Intact padeye.

Table 3

Summary of test results for fatigue crack detection in padeye specimens.

No. of tests		ADI	Test result
Test #1	Damaged padeye	2.17e-12 8.43e-12 1.22e-11 2.52e-11	$ADI > 0$ Damage
	Intact padeye	-8.33e-14 -5.56e-14 -3.87e-14 -2.88e-14	$ADI < 0$ Intact
	Damaged padeye	3.33e-12 2.30e-11 1.01e-11 1.81e-11	$ADI > 0$ Damage
	Intact padeye	-6.44e-14 -6.47e-14 -5.14e-14 -1.34e-14	$ADI < 0$ Intact
Test #2	Damaged padeye	4.51e-10 1.43e-10 3.76e-10 1.18e-9	$ADI > 0$ Damage
	Intact padeye	-3.53e-13 -6.78e-14 -5.10e-15 -6.12e-15	$ADI < 0$ Intact
	Damaged padeye	4.51e-10 1.43e-10 3.76e-10 1.18e-9	$ADI > 0$ Damage
	Intact padeye	-3.53e-13 -6.78e-14 -5.10e-15 -6.12e-15	$ADI < 0$ Intact
Test #3	Damaged padeye	4.51e-10 1.43e-10 3.76e-10 1.18e-9	$ADI > 0$ Damage
	Intact padeye	-3.53e-13 -6.78e-14 -5.10e-15 -6.12e-15	$ADI < 0$ Intact

(ADAM) optimizer [32]. The mini-batch size for the proposed technique was determined considering the lower-limit frequency, which is the difference in the modulation frequency at $f_b - f_a$ in this research. To effectively learn the sequential patterns, the signal length in the

Table 4

Comparison of the diagnosis result between proposed method and conventional method at test #1.

	Proposed method	Conventional method
Damaged padeye	$ADI > 0$	Confidence level (%)/No. of outliers 99.9%/3 99.99%/2 99.999%/0
Diagnosis	Damage	Damage Damage Intact (False alarm)
Intact padeye	$ADI < 0$	Confidence level (%)/No. of outliers 99.9%/5 99.999%/3 99.999%/2
Diagnosis	Intact	Damage Damage (False alarm) Damage (False alarm)

Table 5

Results of DLSTM network architecture optimization for real operating bridge.

Layer	Hidden units	Batch size	Batch loss	Validation loss	Epochs
3	[150, 100, 100]	500	0.0044	0.0024	720
3	[150, 150, 100]	500	0.0046	0.0026	640
3	[200, 150, 100]	500	0.0040	0.0023	800
3	[200, 200, 100]	500	0.0040	0.0024	800
4	[150, 100, 100, 100]	500	0.0040	0.0024	880
4	[150, 150, 100, 100]	500	0.0068	0.0037	480

mini-batch, L_{tr} , was set such that the period of the sequential pattern of the difference modulation could be repeated at least 100 times in the mini-batch, as follows:

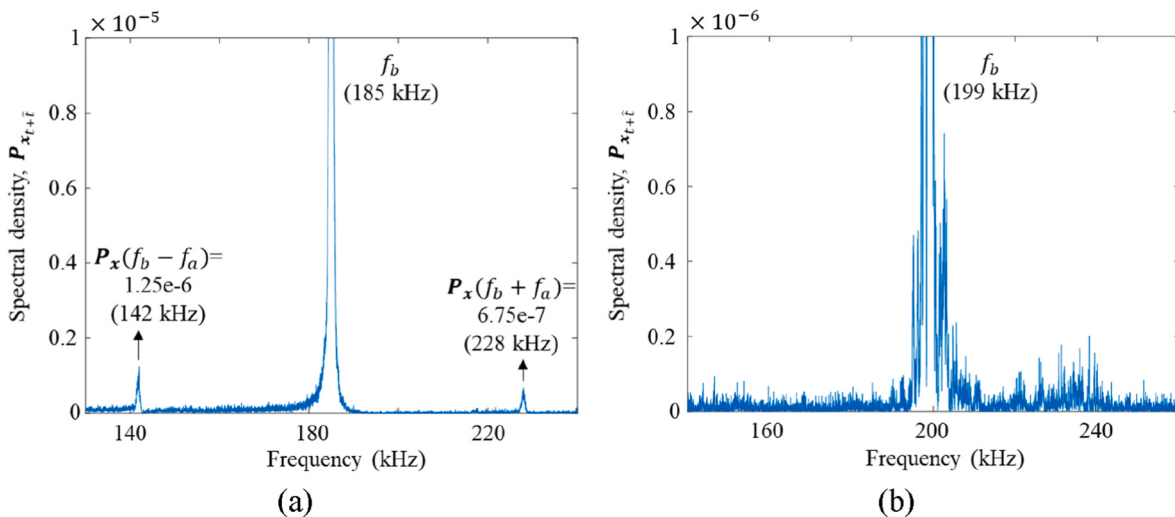


Fig. 11. Representative raw ultrasonic response signals in the frequency domain obtained from real bridge test. (a) Location 1 (Damaged), (b) Location 2 (Intact).

Table 6

Results of fatigue crack detection of real operating bridge.

n	$t + \hat{t}$	$(P_{x_{t+\hat{t}}} \sim (f_b - f_a) P_{x_{t+\hat{t}}} \sim (f_b + f_a))_n$	
		Location 1	Location 2
1	0.12	6.18e-11	2.15e-15
2	0.19	3.64e-10	1.37e-15
3	0.26	4.72e-10	9.54e-16
4	0.33	8.12e-10	7.00e-16
5	0.40	1.30e-9	5.36e-16
<i>ADI</i>		4.32e-9 <i>ADI</i> > 0	-1.11e-14 <i>ADI</i> < 0
		1.54e-9	-5.94e-15
		4.86e-9	-3.63e-15
		6.97e-9	-2.34e-15

$$L_{tr} = \frac{1}{f_b - f_a} \times 100 \quad (16)$$

$$ADI = \frac{d(P_{x_{t+\hat{t}}} \sim (f_b - f_a) P_{x_{t+\hat{t}}} \sim (f_b + f_a))}{d(t + \hat{t})} \approx \frac{\Delta(P_{x_{t+\hat{t}}} \sim (f_b - f_a) P_{x_{t+\hat{t}}} \sim (f_b + f_a))}{\Delta(t + \hat{t})} = \frac{(P_{x_{t+\hat{t}}} \sim (f_b - f_a) P_{x_{t+\hat{t}}} \sim (f_b + f_a))_{n+1} - (P_{x_{t+\hat{t}}} \sim (f_b - f_a) P_{x_{t+\hat{t}}} \sim (f_b + f_a))_n}{\rho} \quad (18)$$

Then, the optimal mini-batch size was calculated as:

$$\text{Mini batch size} \geq L_{tr} \times FS = \frac{FS}{f_b - f_a} \times 100 \quad (17)$$

where FS is the sampling rate.

Hyperparameter studies were performed to optimize the DLSTM network architecture by varying the numbers of stacked layers and hidden units. The minibatch size was 500. To avoid overfitting, dropout was introduced in each LSTM layer, and the dropout factor was set to 0.2. The learning rate was set as 0.0005. The DLSTM network training and validation were performed in a MATLAB (R2019a) environment on a personal computer with an Intel Core i7-9700 @ 3-GHz CPU, 16 GB RAM, and an NVIDIA GeForce RTX 2060 GPU.

The results of the optimal hyperparameters are presented in Table 1. The optimal architecture was selected by considering the minimum validation loss. The number of stacked layers and hidden units were finalized as 3 and [150, 150, 100], respectively.

4.3. Results of fatigue crack detection

Fig. 8 shows two representative ultrasonic response signals obtained from the damaged and intact padeyes in Test #1. It is difficult to identify the nonlinear modulation components because of the high noise level considering the long cable linking the PZTs, data measurement system, and leakage of ultrasonic energy into the water. Because the density difference between water and steel is relatively less than that between air and steel, more ultrasonic energy is leaked into the water than in air. In short, ultrasonic waves can leak into water during the wave propagation, so the amplitude of the ultrasonic waves is weakened and the signal-to-noise ratio decreases accordingly.

Table 2 presents the representative test results acquired from the damaged and intact padeyes in Test #1. For ultrasonic prediction using the trained DLSTM, the time interval ρ was calculated as 0.09 s, and n was considered up to 5 ($n = 1, 2, \dots, 5$). The proposed *ADI* was calculated using the discrete-time rate of change estimated at each n as follows:

For the damaged padeye specimen, the *ADI* value was always positive; thus, the fatigue crack was successfully detected. However, no cracks were detected in the intact padeye specimen because the *ADI* was calculated as negative, as listed in Table 2. Additionally, Fig. 9 shows a representative $x_{t+\hat{t}}$ from the damaged specimen when $n = 1$, and Fig. 10 plots $P_{x_{t+\hat{t}}}$ calculated at three different time intervals ($t + \hat{t} = 0.14, 0.32, 0.50$ s) from both the damaged and intact specimens in Test #1.

An identical test was repeated thrice to examine the reliability of the proposed technique, and the test results are summarized in Table 3. Fatigue cracks were successfully detected in all three tests, and all *ADI*s were less than zero for the intact specimen.

Table 4 shows a comparison of the crack diagnosis results of Test #1 using the proposed method and a conventional reference-free damage detection method [18]. The conventional reference-free damage detection method detects the crack by outlier analysis to find the nonlinear ultrasonic modulation components that exceed the confidence level (threshold) of the current noise level. In the damaged case, the proposed

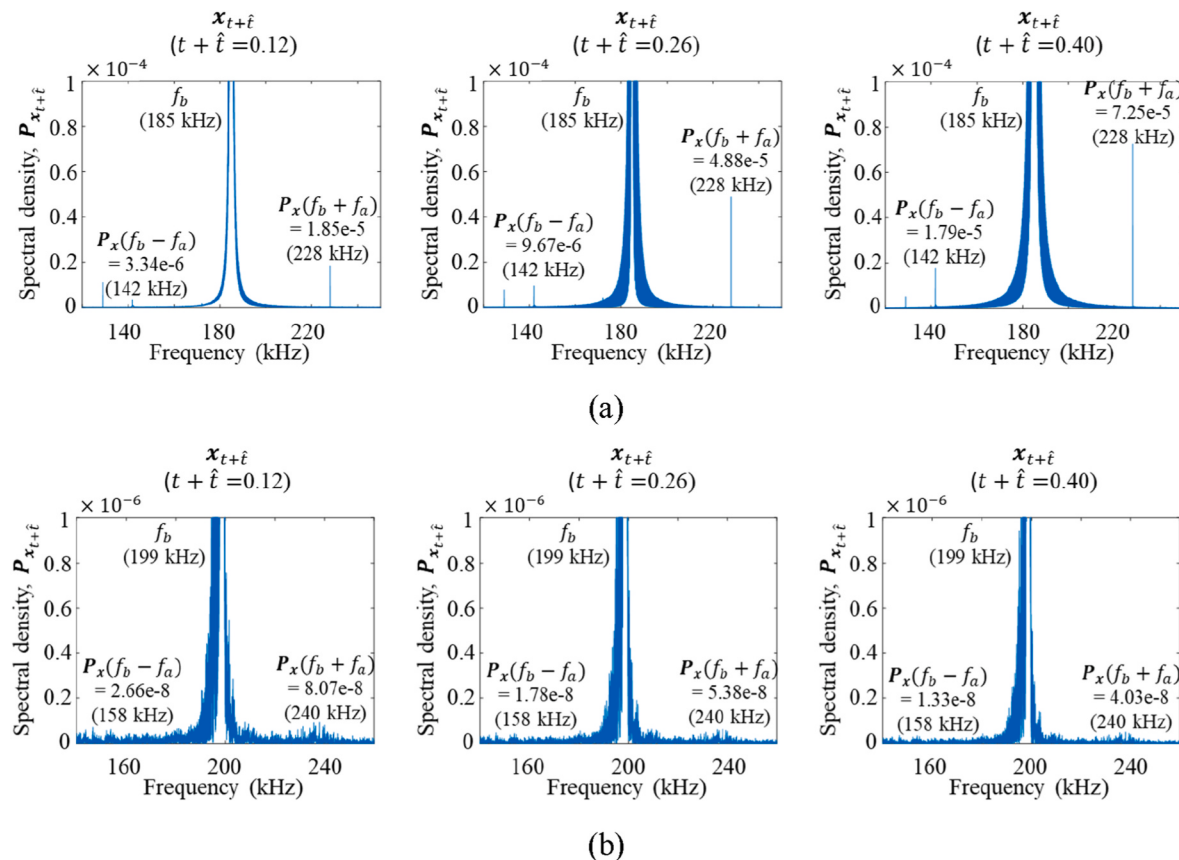


Fig. 12. Representative $P_{x_{t+̂}}$ calculated at three different time intervals ($t + \hat{t} = 0.12, 0.26, 0.40$). (a) Location 1 (Damaged), (b) Location 2 (Intact).

method successfully detected the crack, but the conventional method made a false alarm at the 99.999% confidence level. In the intact case, no cracks were detected by the proposed method, but false alarms occurred by the conventional method in all three confidence levels due to noise interference. Conclusively, the proposed method secures the consistency of the diagnosis because the proposed method does not rely on the user-specified threshold.

5. Experimental validation using data obtained from a real bridge

5.1. Test configuration

The proposed technique was further applied to the data obtained from a real long-span bridge. The target bridge was a long-span bridge near Seoul, Republic of Korea, linking the South Korean Peninsula and an island. The bridge has been exposed to unexpected heavy traffic loads for several years, and fatigue cracks have been identified at several locations. Because of the confidentiality agreement with the bridge authority, the identity and details of the bridge are not revealed here, and only limited outcomes of the fatigue crack detection tests are reported in this study.

All experimental setups for the bridge test were identical to those of the previous SFT test, unless described differently. For monitoring the fatigue crack, a triple PZT module [33] developed by the authors' research group was adopted for ultrasonic measurement. Each triple PZT module consists of three identical PZTs packaged by Kapton tape with a printed circuit, the modules were installed near the welded joints inside the box girder where most fatigue cracks occur. The input frequency combination was determined considering the frequency response at the target location. The local resonance frequencies were selected because they can lead to larger ultrasonic responses in large structures. In

addition, the low and the high frequencies were determined in the ranges of 40–70 kHz and 150–220 kHz, respectively, considering the operation bandwidth of PZTs and the sampling rate of the data acquisition system. Ultrasonic data obtained from one damaged location (Location 1) and one intact location (Location 2) were used for validation. Ultrasonic inputs at 43 kHz (f_a) and 185 kHz (f_b) were applied to Location 1, and those at 41 kHz (f_a) and 199 kHz (f_b) were applied to Location 2.

5.2. DLSTM network construction, training, and optimization

The training process for the bridge test was identical to that for the SFT test. The results of the optimization of the hyperparameters are summarized in Table 5. The optimal number of stacked layers and hidden units were selected as 3 and [200, 150, 100], respectively.

5.3. Test results

Fig. 11 shows two ultrasonic response signals obtained from Locations 1 and Location 2. Nonlinear ultrasonic modulation components appeared in the signal measured at Location 1. Table 6 presents the test results for the two selected locations. n was considered up to 5 ($n = 1, 2, \dots, 5$), and ρ was calculated as 0.07 s in this experiment. The ADI values in Table 5 verified that the ADI became positive at Location 1 with fatigue cracks, while it remained negative for Location 2. Again, Fig. 12 plots $P_{x_{t+̂}}$ calculated at three representative time intervals ($t + \hat{t} = 0.12, 0.26$, and 0.40 s) for Locations 1 and 2.

6. Conclusions

In this study, a reference-free fatigue crack detection technique using

a deep long short-term memory network (DLSTM) and nonlinear ultrasonic modulation was developed. An ultrasonic signal is obtained from the target structure, and then a DLSTM network is trained to learn the repeated sequential pattern of the ultrasonic signal. The following sequence of ultrasonic signals was forecasted, and the absolute damage index (*ADI*) was calculated using the measured and forecasted ultrasonic signals. A fatigue crack was detected when the *ADI* value was positive. The proposed technique was applied to ultrasonic data obtained from a submerged floating tunnel (SFT) model and a real bridge. The fatigue crack of the anchor system for the SFT model was successfully identified, and the fatigue crack that occurred in the real operating bridge was successfully detected. The uniqueness of this study is as follows: (1) Reference-free crack diagnosis using only current ultrasonic signal without any reference signal obtained from the intact condition; (2) Online instantaneous training of the DLSTM network to extract the inherent sequential features induced by a crack without accumulation of past training data; (3) Automatic crack diagnosis without any user-specified threshold for decision making; and (4) Improved crack detection performance under noisy under-water and real field environments.

Currently, this research does not investigate the effects of temperature variations on the measured ultrasonic signal and the proposed *ADI* for further estimation of the remaining fatigue life. The following research explores the application of the proposed technique to real bridge monitoring under various temperature conditions.

Author statement

1. Jinho Jang: Conceptualization, Methodology, Formal analysis, Writing, Experiment.
2. Peipei Liu: Supervision, Paper review & editing.
3. Ohjun Kwon: Experiment.
4. Jaemook Choi: Experiment.
5. Zhanxiong Ma: Experiment.
6. Hoon Sohn: Supervision, Paper review & editing, Project administration.

Declaration of competing interest

The authors declare that they have no known competing financial interests or personal relationships that could have appeared to influence the work reported in this paper.

Data availability

Data will be made available on request.

Acknowledgments

This work was supported by a National Research Foundation of Korea (NRF) grant funded by the Korean government (MSIP) (No. 2017R1A5A1014883).

References

- [1] Campbell S, Richard R, Partridge J. Steel moment frame damage predictions using low-cycle fatigue. In: The 14th world conference on earthquake engineering; 2008.
- [2] Kim J-Y, Jacobs L, Qu J. Nonlinear ultrasonic techniques for nondestructive damage assessment in metallic materials. The 8th International Workshop on Structural Health Monitoring; 2011. p. 531–8.
- [3] Ho S, White R, Lucas J. A vision system for automated crack detection in welds. *Meas Sci Technol* 1990;1:287.
- [4] Zilberstein V, Schlicker D, Walrath K, Weiss V, Goldfine N. MWM eddy current sensors for monitoring of crack initiation and growth during fatigue tests and in service. *Int J Fatig* 2001;23:477–85.
- [5] Maslouhi A. Fatigue crack growth monitoring in aluminum using acoustic emission and acousto-ultrasonic methods. *Struct Control Health Monit* 2011;18:790–806.
- [6] Williams J, Yazzie K, Padilla E, Chawla N, Xiao X, De Carlo F. Understanding fatigue crack growth in aluminum alloys by *in situ* X-ray synchrotron tomography. *Int J Fatig* 2013;57:79–85.
- [7] An Y-K, Kim JM, Sohn H. Laser lock-in thermography for detection of surface-breaking fatigue cracks on uncoated steel structures. *NDT E Int* 2014;65:54–63.
- [8] Liu P, Jang J, Yang S, Sohn H. Fatigue crack detection using dual laser induced nonlinear ultrasonic modulation. *Opt Laser Eng* 2018;110:420–30.
- [9] Cantrell JH, Yost WT. Acoustic harmonic generation from fatigue-induced dislocation dipoles. *Philos Mag A* 1994;69:315–26.
- [10] Liu M, Kim J-Y, Jacobs L, Qu J. Experimental study of nonlinear Rayleigh wave propagation in shot-peened aluminum plates—feasibility of measuring residual stress. *NDT E Int* 2011;44:67–74.
- [11] Liu P, Sohn H, Kundu T. Fatigue crack localization using laser nonlinear wave modulation spectroscopy (LNWMS). *J Korean Soc Nondestruct Test* 2014;34:419–27.
- [12] Kim Y, Lim HJ, Sohn H. Nonlinear ultrasonic modulation based failure warning for aluminum plates subject to fatigue loading. *Int J Fatig* 2018;114:130–7.
- [13] Donskoy D, Sutin A, Ekimov A. Nonlinear acoustic interaction on contact interfaces and its use for nondestructive testing. *NDT E Int* 2001;34:231–8.
- [14] Donskoy DM, Sutin AM. Vibro-acoustic modulation nondestructive evaluation technique. *J Intell Mater Syst Struct* 1998;9:765–71.
- [15] Jang J, Liu P, Kim B, Kim S-W, Sohn H. Silicon wafer crack detection using nonlinear ultrasonic modulation induced by high repetition rate pulse laser. *Opt Laser Eng* 2020;129:106074.
- [16] Jeon I, Lim HJ, Liu P, Park B, Heinze A, Sohn H. Fatigue crack detection in rotating steel shafts using noncontact ultrasonic modulation measurements. *Eng Struct* 2019;196:109293.
- [17] Parsons Z, Staszewski WJ. Nonlinear acoustics with low-profile piezoceramic excitation for crack detection in metallic structures. *Smart Mater Struct* 2006;15:1110.
- [18] Lim HJ, Sohn H, DeSimio MP, Brown K. Reference-free fatigue crack detection using nonlinear ultrasonic modulation under various temperature and loading conditions. *Mech Syst Signal Process* 2014;45:468–78.
- [19] Achenbach J. Wave propagation in elastic solids. Elsevier; 2012.
- [20] Sampath S, Jang J, Sohn H. Ultrasonic Lamb wave mixing based fatigue crack detection using a deep learning model and higher-order spectral analysis. *Int J Fatig* 2022;163:107028.
- [21] De Lima W, Hamilton M. Finite-amplitude waves in isotropic elastic plates. *J Sound Vib* 2003;265:819–39.
- [22] Van Den Abeele K-A, Johnson PA, Sutin A. Nonlinear elastic wave spectroscopy (NEWS) techniques to discern material damage, part I: nonlinear wave modulation spectroscopy (NWMS). *J Res Nondestruct Eval* 2000;12:17–30.
- [23] Jin Z, Yang Y, Liu Y. Stock closing price prediction based on sentiment analysis and LSTM. *Neural Comput Appl* 2020;32:9713–29.
- [24] Oliveira DD, Rampinelli M, Tozzato GZ, Andreão RV, Müller SM. Forecasting vehicular traffic flow using MLP and LSTM. *Neural Comput Appl* 2021;33:17245–56.
- [25] Gers FA, Schmidhuber J, Cummins F. Learning to forget: continual prediction with LSTM. *Neural Comput* 2000;12:2451–71.
- [26] LeCun Y, Bengio Y, Hinton G. Deep learning. *Nat* 2015;521:436–44.
- [27] Chung J, Kastner K, Dinh L, Goel K, Courville AC, Bengio Y. A recurrent latent variable model for sequential data. *Adv Neural Inf Process Syst* 2015:28.
- [28] Sagheer A, Kotb M. Time series forecasting of petroleum production using deep LSTM recurrent networks. *Neurocomputing* 2019;323:203–13.
- [29] Utgoff PE, Stracuzzi DJ. Many-layered learning. *Neural Comput* 2002;14:2497–529.
- [30] Boullaut L, Sidahmed M. Cyclostationary approach and bilinear approach: comparison, applications to early diagnosis for helicopter gearbox and classification method based on HOCS. *Mech Syst Signal Process* 2001;15:923–43.
- [31] Lim HJ, Sohn H, Liu P. Binding conditions for nonlinear ultrasonic generation unifying wave propagation and vibration. *Appl Phys Lett* 2014;104:214103.
- [32] Kingma DP, BaAdam J. A method for stochastic optimization. *arXiv preprint arXiv*; 2014. 1412.6980.
- [33] Lim HJ, Kim Y, Sohn H, Jeon I. Reliability improvement of nonlinear ultrasonic modulation based fatigue crack detection using feature-level data fusion. *Smart Struct Syst* 2017;20:683–96.